TECHNICAL PAPER

# Improvement of Metallurgical and Mechanical Properties of Gas Tungsten arc Weldments of Alloy 686 by Current Pulsing

**B. Arulmurugan[1,2] · M. Manikandan[1]**

**Abstract** This research article examines the metallurgical and mechanical behavior of twenty-first-century nickel-based superalloy 686. The weld joints were produced with ERNiCrMo-4 and ERNiCrMo-14 filler wires by continuous current gas tungsten arc welding (GTAW) and pulsed current gas tungsten arc welding (PCGTAW) mode. Optical and scanning electron microscope (SEM) analyses were performed to evaluate the microstructure of welded joints. PCGTAW weldments showed refined microstructure, narrower weld bead and minimum heat-affected zone compared to GTAW. SEM analysis revealed the presence of secondary phases in the interdendritic regions of GTA and PCGTA weldments made of ERNiCrMo-4 and GTA ERNiCrMo-14 fillers. Energy-dispersive X-ray spectroscopy examination was also performed to assess the microsegregation of alloying elements in the weldments. The results proved nonexistence of microsegregation in the case of PCGTA weldments made by ERNiCrMo-14 filler. However, segregation of alloying element Mo was noticed in other weldments. Strength and toughness of the weld joints were evaluated by conducting tensile and Charpy impact tests. The refined microstructure with the absence of microsegregation obtained in the PCGTA welding made with ERNiCrMo-14 filler wire resulted in the higher strength and toughness than other weldments.

✉ M. Manikandan
   mano.manikandan@gmail.com

   B. Arulmurugan
   enggarul@gmail.com

1   School of Mechanical Engineering, VIT, Vellore 632014, India

2   KPR Institute of Engineering and Technology, Coimbatore 641407, India

## 1 Introduction

Alloy 686 (UNS N06686) is a solid-solution-strengthened nickel-based superalloy resulting from Ni–Cr–Mo ternary system. It is the most highly corrosion-resistant alloy commercially available today [1]. This alloy offers outstanding corrosion resistance in oxidizing, reducing and mixed acid environments. It was developed in the year 1992 by Special Metals Corporation to provide superior corrosion resistance than the traditionally used alloys C-276 and C-22 [2]. Chromium (Cr) enhances better corrosion resistance in the oxidizing environment, whereas molybdenum (Mo) supports and maintains corrosion resistance in the reducing environments. Molybdenum and tungsten (W) assist in resistance to localized corrosion such as pitting [3–5]. The presence of low carbon (0.01%) aids in minimization of grain boundary precipitation and preserves corrosion resistance in the heat-affected zone (HAZ) of the weldment.

The alloy 686 has a wide range of applications in the industries such as marine, chemical processing and air pollution control [flue gas desulfurization (FGD)]. In the FGD system, alloy 686 is widely used in the most severe environments encountered in the stack liners, ducts, dampers, scrubbers and stack gas reheaters [5].

The premature failure in the weldment of solid-solution-strengthened Ni–Cr–Mo alloys is caused by the potential formation of intermetallic topologically closed packed (TCP) phases such as $\sigma$, $\mu$ and $P$ at the end of solidification in the fusion zone [6]. This is because of the intentional

addition of more number of alloying elements to improve the properties which exceed the solubility limit during the eutectic reaction. The Ni–Cr–Mo composition has Mo proportion which is less than 15% of weight, and very less percentage of iron and tungsten altogether solidifies as a single-phase austenite which resists the formation of brittle TCP phase. The Mo content increases more than the above value, which noticeably shows the formation of TCP phases, which could not be eliminated [6, 7].

The TCP phases are brittle in nature because of their limited slip system which deteriorates material's ductility and toughness and makes them unsuitable for high-strength applications [6]. These secondary phases are formed at interdendritic regions and weaken the dendrite core through the reduction of Cr, Mo contents in the austenite matrix. Higher amount of Mo present in the interdendritic region causes the formation of $\mu$ and $P$ phases, and high Cr content leads to the formation of $\sigma$ phase [7].

Arc welding is an essential fabrication process which is used for the joining of various products out of this alloy. It is important to study the behavior of alloy 686 by arc welding technique. Of various arc welding techniques, gas tungsten arc welding (GTAW) is a promising method to fabricate Ni–Cr–Mo welds economically. The major problem associated with the welding of Ni–Cr–Mo-based superalloys is the formation of intermetallic phases due to microsegregation of alloying elements. Microsegregation in the weldment is the root cause of the problem, and it can be diminished by judicious selection of the welding process and parameters [8]. This widespread welding issue in Ni–Cr–Mo alloys can be effectively mitigated by increasing the cooling rate during solidification. It can be attained by pulsed current (PC) mode in arc welding and high-density welding processes. In general, arc welding technique with the pulsed current mode is more economical than the high beam welding processes, because they are costlier and associated with issues like reflection and vacuum generation.

Pulsed current gas tungsten arc welding (PCGTAW) varies specifically in heat supply, compared to constant current gas tungsten arc welding (GTAW). In GTAW, heat supply to the material is continuous throughout the cycle, so it affects the vicinity, thus leading to wider HAZ, and increases the solidification time and results in poor weld quality. On the other hand, PCGTAW supplies energy to the two cycles through peak and base currents. The peak current predominantly melts the core material and performs welding operation. Energy supply is absent during base current, which aids in solidification of the weld metal. In contrast to GTAW, the PCGTAW supplies the heat energy intermittently in a periodic cycle, allowing the material to have effective cooling rate and reduces the time to solidify which improves the quality of the weld.

It is believed that the extent of microsegregation may be brought down by proper selection of filler wire. In general, base metal composition filler wire is widely used in the industrial practice [9]. In the present study, filler wire ERNiCrMo-14 with essential composition that nearly matches with base metal has been chosen and also weldments have been fabricated with ERNiCrMo-4. Since the alloy 686 is derived from alloys C-276 and C-22, significant weldability characteristics of the filler wire ERNiCrMo-4 are expected to be inhibited in alloy 686 as well [2]. The same authors have already investigated the welding of alloy 686 with ERNiCrMo-10 (matching composition of alloy C-22) and autogenous mode [10].

The following literature has well documented the welding behavior and thermal stability of various Ni–Cr–Mo-based superalloys; details are given in the following paragraphs.

Cieslak et al. [11] investigated the weldability of five different Ni–Cr–Mo-based super alloys (alloys C-4, C-22, C-276, 625 and 718) using arc welding technique. The authors noticed the formation of TCP phases such as $\sigma$, μ, $P$ and Laves in the different weldments. The authors reported the formation of $P$ and $\mu$ in the alloys C-276 and C-22 and that the segregation of alloying elements during solidification is widely responsible for the observed TCP phases. These TCP phases lead to hot cracking in the fusion zone. In another study conducted by Perricone and DuPont [12], the effect of composition on the solidification behavior of several Ni–Cr–Mo and Fe–Ni–Cr–Mo alloys was reviewed. The authors observed that there is no evidence found of the occurrence of $P$ and μ phases in the weldment containing 12 wt.% Mo content, but upon increasing Mo content, formation of Mo-rich secondary phase ($P$, $\mu$) in the microstructure is noticed. In addition, Zheng [13] reported that high concentration of Mo and W in Ni–Cr–Mo alloys leads to the occurrence of TCP phases ($P$ and μ) during solidification.

Silva et al. [7] studied the microstructure characteristics of dissimilar weld overlays with alloy 686 deposited on C–Mn steel plates using SEM, TEM, chemical mapping and X-ray diffraction analysis. The authors found the formation of $P$, $\sigma$ and μ intermetallic phases at the end of the solidification and identified that these phases are prone to hot cracking.

Gallagher and Lippold [14] investigated the formation of secondary phases using Scheil simulation analysis in alloy C-22, and they identified that there is a positive exponential relationship between combined Mo + W level and secondary phase formation.

It is evident from the literature that the formation of TCP phases adversely affects the weldability and other properties of interest in Ni–Cr–Mo-based superalloys. The following few studies documented that higher cooling rate achieved in the pulsed current gas tungsten arc welding cut down the extent of microsegregation by minimizing secondary TCP phases formation and also the improvement of

metallurgical characteristics and mechanical properties of weld joints in different grades of Ni-based superalloys.

Manikandan et al. [15] compared the continuous and pulsed current gas tungsten arc welding of alloy 718. The authors concluded that the faster cooling rate achieved in pulsed current mode results in improved mechanical properties of the weld joint with reduction of Laves phase in the fusion zone.

Manikandan et al. [8, 16] investigated the welding of alloy C-276 by GTAW and PCGTAW with autogenous mode and different filler wires. The authors concluded that pulsed current gas tungsten arc welding shows refined microstructure with reduced microsegregation with improved mechanical properties compared to continuous current gas tungsten arc welding technique. The authors also reported that improper selection of filler wire leads to higher segregation in both welding techniques.

Janaki Ram et al. [17] exploited the significance of pulsing of welding current and reported that there is a reduced segregation of niobium (Nb) and interconnectivity of Laves network which has resulted in improved stress rupture properties.

Farhani et al. [18] compared the quality of weld joints fabricated with GTAW and PCGTAW in alloy 617. Authors observed the refined microstructure and improved mechanical properties in the PCGTAW compared to GTAW.

Arulmurugan and Manikandan [10] compared the welding of alloy 686 with GTAW and PCGTAW techniques in autogenous mode and ERNiCrMo-10 filler wire. The authors found that PCGTAW with ERNiCrMo-10 shows the absence of microsegregation compared to other welding techniques. PCGTAW in autogenous mode and with ERNiCrMo-10 filler wire shows improved mechanical properties compared to GTAW technique.

Based on the reported literature, authors realized the need for studying the welding of alloy 686 with base metal composition filler wire. Hitherto, there is no literature reported on the alloy 686 fabricated with GTAW and PCGTAW with ERNiCrMo-4 and ERNiCrMo-14 filler wires. The objective of the present study is to evaluate the welding behavior of alloy 686 with different filler wires and the possible extent to diminish the microsegregation of alloying elements to cut down the formation of secondary phases. The results obtained in the present research work will be highly beneficial to the industries working in the alloy 686.

## 2 Materials and Methods

### 2.1 Material and Welding Procedure

Solution-annealed 3-mm-thick hot-rolled sheet of alloy 686 was procured, and its chemical composition was cross-

checked and confirmed with optical emission spectroscopy. The test result is listed in Table 1. The weld coupons were prepared in the dimensions of 130 mm × 55 mm × 3 mm with wire-cut electric discharge machine (EDM), and the surfaces were cleaned with acetone. Welding trials were carried out manually in both continuous and pulsed modes using KEMPI DWE 400 machine. The process parameters employed in the present study are listed in Table 2. Figure 1a–d represent the weld joints (face and root) fabricated by GTAW and PCGTAW. The joints were fabricated with the filler wires ERNiCrMo-4 and ERNiCrMo-14. The filler wire chemical composition is also listed in Table 1. Standard V-butt configurations which incorporate single V-groove having a root gap of 1 mm and include an angle of 60° were employed for joining GTA and PCGTA weldments. The filler rod of diameter 1.6 mm was used to fill the V-groove in butt weld joints. In order to shield the molten metal and enable the stability of arc, argon was used as the shield gas with a flow rate of 15 L/min. The total heat input supplied to fabricate GTAW and PCGTA weldments was calculated by using Eqs. (1), (2) and (3).

Total heat input supplied to fabricate GTAW was determined by using Eq. (1),

$$H = \frac{I \times V}{S} \times \eta \text{ in } \left( \frac{\text{kJ}}{\text{mm}} \right) \tag{1}$$

The total heat input supplied to fabricate PCGTAW was calculated by using Eqs. (2) and (3),

$$I_{\text{m}} = \frac{(I_{\text{p}} \times t_{\text{p}}) + (I_{\text{b}} \times t_{\text{b}})}{(t_{\text{p}} + t_{\text{b}})} \text{in amps} \tag{2}$$

$$H = \frac{I_{\text{m}} \times V}{S} \times \eta \text{ in } \left( \frac{\text{kJ}}{\text{mm}} \right) \tag{3}$$

where $I$ represents current in amps, $I_{\text{m}}$ represents mean current in amps, $I_{\text{p}}$ is pulse current, amps; $I_{\text{b}}$ background current, amps; $t_{\text{b}}$ background current duration, ms; $t_{\text{p}}$ pulse current duration, ms; $S$ welding speed, mm/min; $V$ voltage, V; $\eta$ efficiency of the welding process. For the GTAW and PCGTAW processes, arc efficiency ($\eta$) was taken as 70% [16].

### 2.2 Metallography and Microstructure Characterization

After the welding process, welded plates were sliced into various sections along their transverse cross section to carry out metallographic characterization. The weld coupon was the integration of base metal, heat-affected zone and fusion zone. The samples were polished manually with silicon carbide (SiC) grit paper ranging from 220 to 2000, and then 0.5-μm alumina powder polishing was carried out. Final polishing was done with water to obtain the mirror

**Table 1** Chemical composition of alloy 686 and filler wires ERNiCrMo-4 and ERNiCrMo-14

| Base/filler metal | Chemical composition (% Wt.) | | | | | | | | |
|---|---|---|---|---|---|---|---|---|---|
| | Ni | Mo | Cr | W | Mn | Fe | S | Co | Others |
| Alloy 686 | Bal | 15.83 | 19.88 | 3.215 | 0.312 | 0.858 | 0.17 | – | 0.008 (P), 0.076 (Si), 0.005(Ti) 0.01(C) |
| ERNiCrMo-4 | Bal | 16.1 | 16.1 | 3.3 | 0.5 | 5.9 | 0.001 | 0.4 | 0.01 (P), 0.15 (Cu), 0.02 (Si) 0.01(C) 0.15 (Vd) |
| ERNiCrMo-14 | Bal | 15 | 19 | 3 | 1 | 5 | 0.02 | – | 0.02 (P), 0.5 (Cu), 0.08 (Si) 0.02 (C) 0.25 (Ti) |

**Table 2** Process parameters of GTA and PCGTA weldments

| Types of welding | Current (A) | Voltage (V) | Peak current (A) | Background current (A) | Pulse frequency (Hz) | Pulse on time | Welding speed (mm/s) | Heat input (kJ/mm) |
|---|---|---|---|---|---|---|---|---|
| GTAW-ERNiCrMo-4 | 120 | 12 | – | – | – | – | 2.1 | 0.976 |
| GTAW-ERNiCrMo-14 | 120 | 12 | – | – | – | – | 2.25 | 0.907 |
| PCGTAW-ERNiCrMo-4 | – | – | 120 | 60 | 6 | 50% | 2.18 | 0.692 |
| PCGTAW-ERNiCrMo-14 | – | – | 120 | 60 | 6 | 50% | 2.26 | 0.668 |
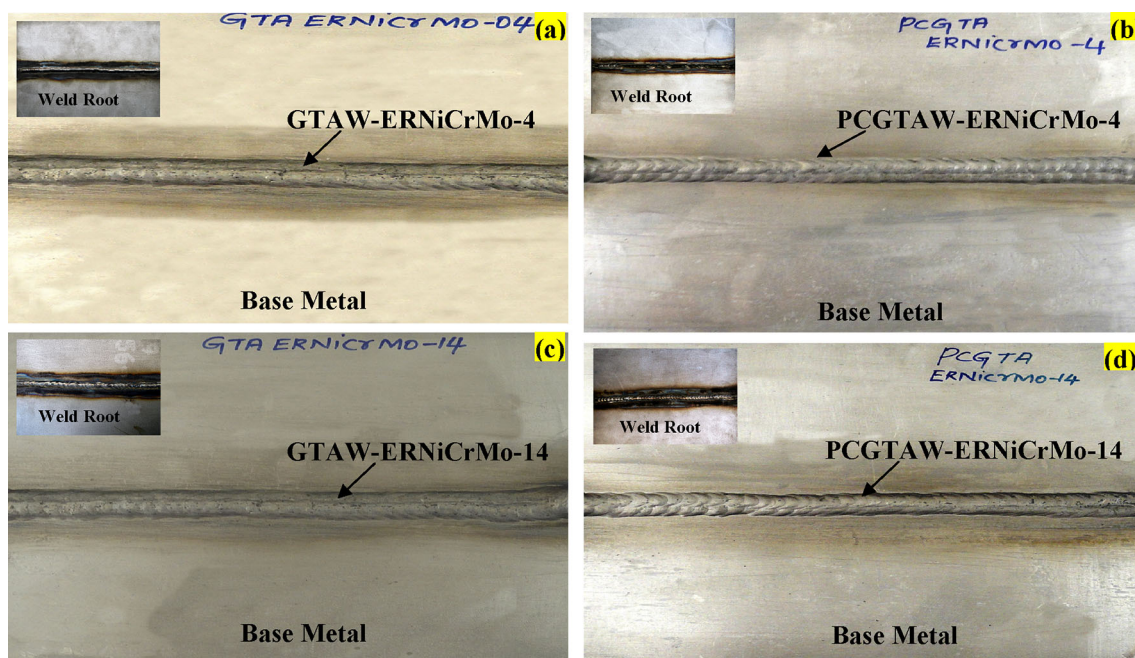


**Fig. 1** Photographic images of weldment made with **a** GTAW-ERNiCrMo-4; **b** PCGTAW-ERNiCrMo-4; **c** GTAW-ERNiCrMo-14; and **d** PCGTAW-ERNiCrMo-14

finish. To reveal the microstructure of base metal (BM), HAZ and fusion zone, the samples were etched with electrolytic etching (10% wt. chromic acid solution) at 12V for 15–20 s. The etched samples' microstructure was examined and captured with optical and scanning electron microscope (SEM). To evaluate the microsegregation of alloying elements, energy-dispersive X-ray spectroscopy

(EDS) analysis was performed in the matrix and inter-dendritic region of weldments.

## 2.3 Mechanical Characterization

The welded samples were characterized to assess the strength, ductility and toughness through tensile and impact
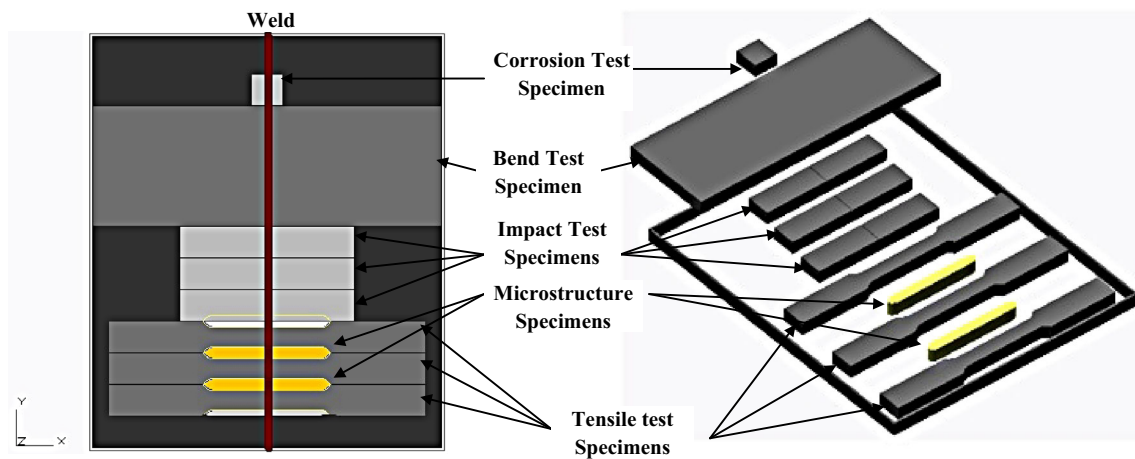
**Fig. 2** Layout of test samples sliced from welded plate

tests in ambient condition. The schematic of the weld joint design is shown in Fig. 2. The tensile test provided the information about the strength and ductility of the welded joints. Universal testing machine (Instron 8801) attached with extensometer was used to carry out the tensile test. The coupons were sliced as per ASTM E8/E-8 M-13a (subsize) standard. Three test trials were performed at a strain rate of 2 mm/min.

Charpy V-notch impact test was conducted to assess the toughness of the weld joints. Test coupons were sliced as per ASTM E-23 standard. SEM fractography analysis was performed to identify the mode of failures in both tensile and impact failure samples.

## 3 Results

### 3.1 Macrostructural Examination

The macro-examination has been conducted to assess the quality of the weld joints produced by GTA and PCGTA welding techniques. Figure 3a–d shows the macro-examination of four different joints produced with different filler wires. No defects are identified in the fusion zone and HAZ of the weldments. It is also noticed that both in ERNiCrMo-4 and ERNiCrMo-14 filler wire weldments, the width of the fusion zone in GTAW is higher than in the PCGTAW. Further, narrower width is observed in PCGTAW.

### 3.2 Microstructure Examination

#### 3.2.1 GTAW and PCGTAW with ERNiCrMo-4 Filler Wire

Figure 4 shows the base metal microstructure of alloy 686. It contains fine equiaxed dendrites with clear grain boundaries and also has annealing twins. Figures 5 and 6

represent the microstructure of weld joint fabricated by GTA and PCGTA welding processes with ERNiCrMo-4 filler wire. Figure 5a and b represents the micrograph of weld center and weld interface region of GTA weldment. Columnar dendrites are seen in weld center. Grain coarsening occurs in the HAZ adjacent to the fusion line (Fig. 5b). Width of HAZ is in the range of 210–249 μm. Further unmixed zone is observed at the weld interface.

Figure 6a and b shows the microstructure of different zones of PCGTAW—fusion zone weld center and weld interface, respectively. The fusion zone consists of fine equiaxed dendritic structure as shown in Fig. 6a. Grain coarsening in the HAZ (Fig. 6b) adjacent to fusion line is very less than in the GTAW. The size of HAZ is lesser in PCGTAW (116–138 μm) when compared to GTAW.

#### 3.2.2 GTAW and PCGTAW with ERNiCrMo-14 Filler Wire

The microstructure of weldments fabricated by GTAW and PCGTAW with ERNiCrMo-14 filler wire is shown in Figs. 7 and 8. Figure 7a represents the weld center microstructure, and Fig. 7b shows weld interface microstructure of GTA weldment. The fusion zone consists of columnar dendrites, and minimum grain coarsening is observed in the interface. In this case, width of HAZ is in the range of 196–250 μm.

The different regions of microstructure in PCGTA weldment are shown in Fig. 8. It is observed that the fine equiaxed dendrites are seen in weld center (Fig. 8a). The size of HAZ is less (73–96 μm) as compared to GTAW in the weld interface, which is shown in Fig. 8b.

Fig. 3 Macrostructure images of weld joints: **a** GTAW-ERNiCrMo-4; **b** PCGTAW-ERNiCrMo-4; **c** GTAW-ERNiCrMo-14; and **d** PCGTAW-ERNiCrMo-14
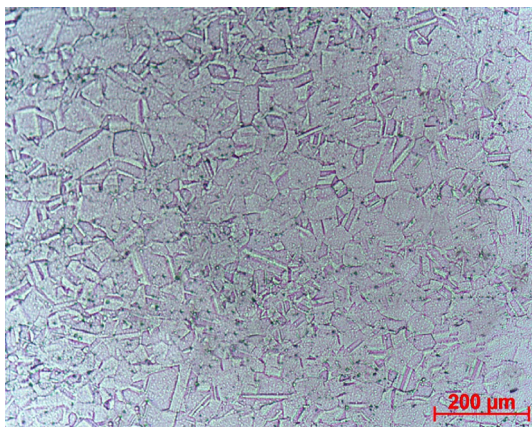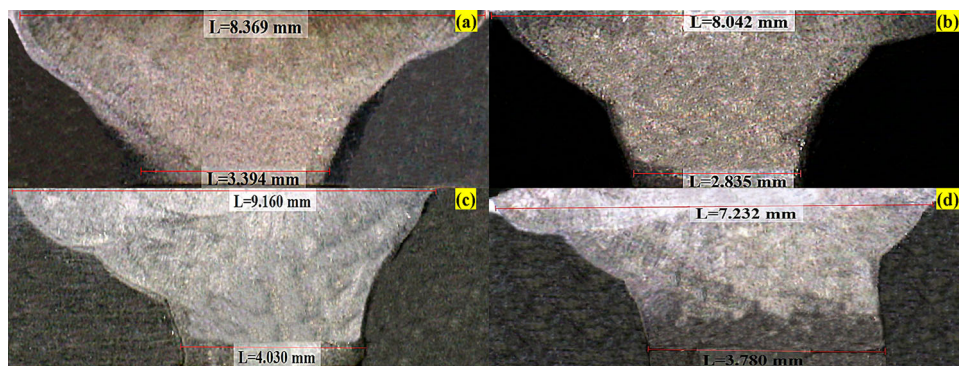




Fig. 4 Optical photograph of base metal microstructure

### 3.3 SEM/EDS Analysis

#### 3.3.1 GTAW and PCGTAW with ERNiCrMo-4 Filler Wire

Figures 9 and 10 depict the SEM/EDS results obtained in GTAW and PCGTAW. The higher-magnification SEM photograph of weld center and weld interface GTA weldment is shown in Fig. 9a and b, whose morphology is observed as columnar dendrite and cellular structure. In both regions, the secondary phases are decorated in the interdendritic regions.

Figure 9i and ii shows the EDS analysis of weld center dendritic core and interdendritic region of GTAW, respectively. Table 3 indicates the collection of elemental values of Ni, Cr, Mo and W at various areas of the weld joint in weight percentage. It can be noticed from Fig. 9i and ii and Table 3 that the interdendritic region is enriched with Mo and to some extent W, but reduced in Ni content compared to the dendritic core. Figure 9iii and iv shows the EDS images of weld interface region, and similar observations are noticed.

Figure 10a and b represent the SEM images of weld center and weld interface of PCGTA weldment. Table 4 contains the compilation of values of Ni, Cr, Mo and W at different regions of the weld joint. Figure 10a indicates weld center SEM micrograph, which contains fine equiaxed dendrite structure. It is noted from the micrograph that secondary phases are decorated in the interdendritic regions like GTAW mode. EDS analysis of weld center dendritic core and interdendritic regions is represented in Fig. 10i and ii. In this case, also the interdendritic region is enriched with Mo and impoverished with Ni. Similar observations are also noticed in the weld interface region (Fig. 10iii and iv).
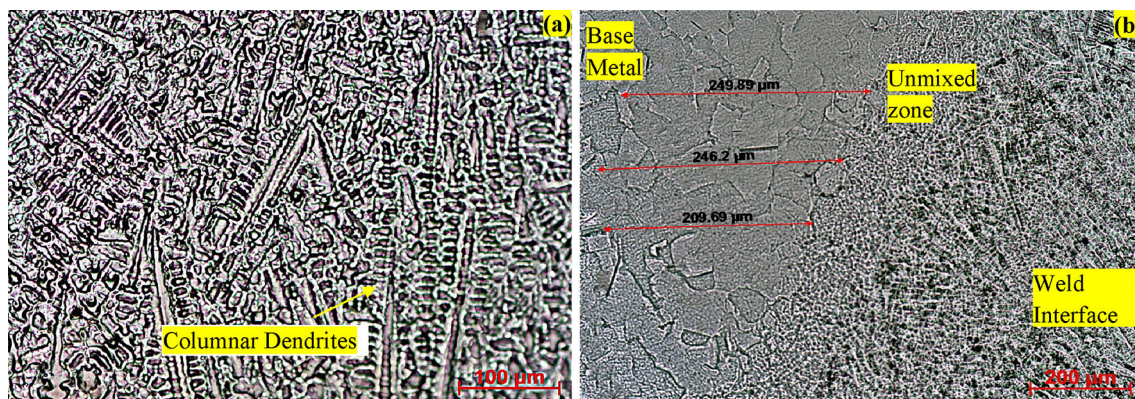


Fig. 5 Optical microstructure of weld joint fabricated by GTAW with ERNiCrMo-4. **a** Fusion zone weld center and **b** weld interface
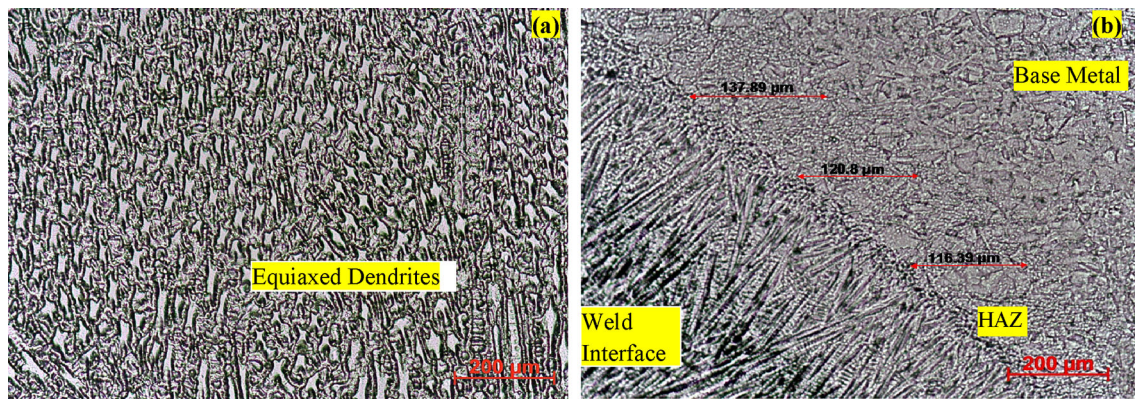
**Fig. 6** Optical microstructure of weld joint produced by PCGTAW with ERNiCrMo-4. **a** Fusion zone weld center and **b** weld interface
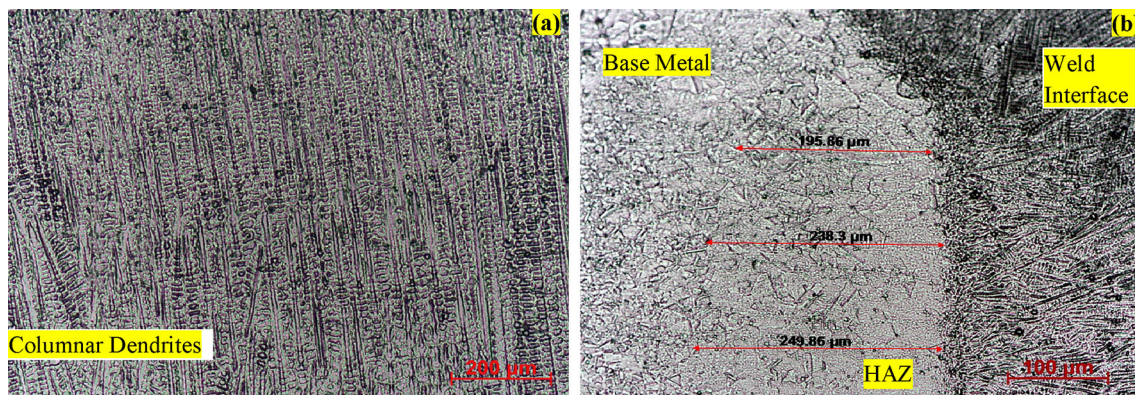


**Fig. 7** Optical microstructure of weld joint produced by GTAW with ERNiCrMo-14. **a** Fusion zone weld center and **b** weld interface
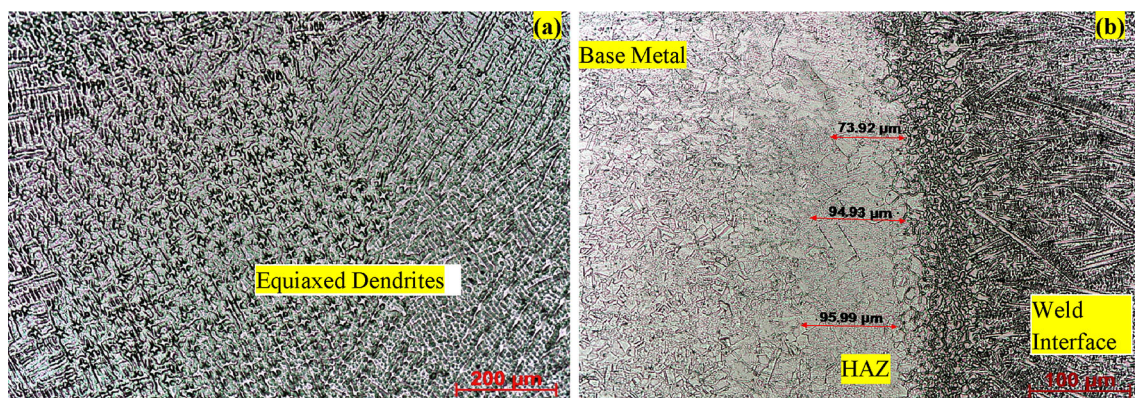


**Fig. 8** Optical microstructure of weld joint fabricated by PCGTAW with ERNiCrMo-14. **a** Fusion zone weld center and **b** weld interface

### 3.3.2 GTAW and PCGTAW with ERNiCrMo-14 Filler Wire

Figure 11a and b illustrate the higher-magnification SEM image of different regions of GTA weldment with filler wire ERNiCrMo-14. Table 5 lists the collection of various quantities of the alloying element at different zones of a weld joint in weight percentage. Fusion zone weld center consists of a cellular structure (Fig. 11a), and in the interface region, columnar dendrites are visible (Fig. 11b). Both weld center and weld interface region are found to be decorated with secondary phase precipitates.

EDS analysis and evaluation of elemental values of fusion zone weld center dendritic core and interdendritic regions of GTAW are shown in Fig. 11i and ii. From Table 5, it is clearly observed that the interdendritic region is rich in Mo and to some extent W content, but poorer in Ni content as compared to the dendritic core. Similar
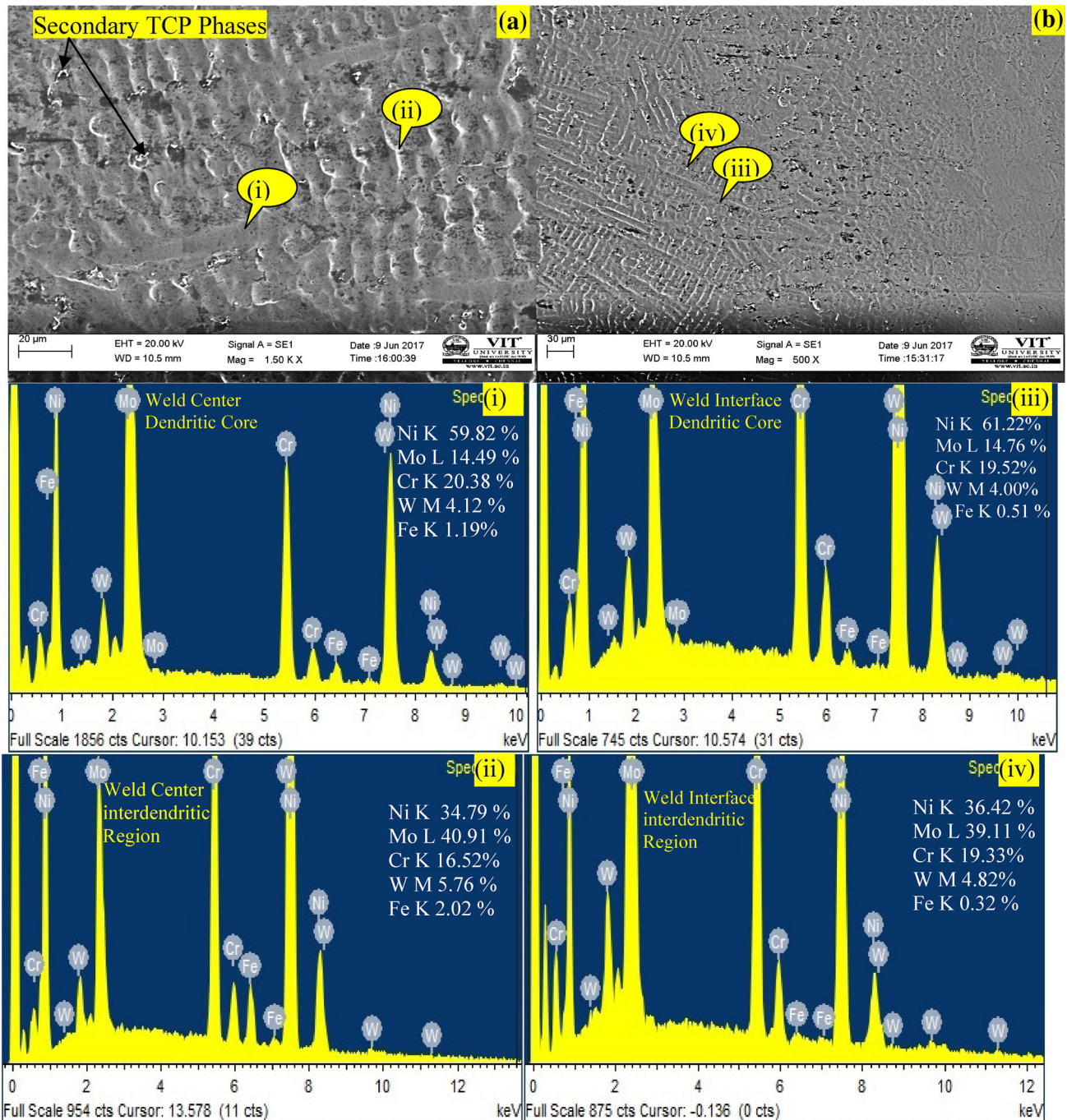
**Fig. 9** SEM/EDS analysis of GTAW-ERNiCrMo-4-welded alloy 686: **a** SEM weld center; **b** SEM weld interface; (i) EDS of weld center dendritic core; (ii) EDS of weld center interdendritic region; (iii) EDS of weld interface dendritic core; and (iv) EDS of weld interface interdendritic region

observations are also noticed in the weld interface region, and it is illustrated in Fig. 11iii and iv.

Figure 12a and b represents the higher-magnification SEM image of weld center and interface regions of PCGTA weldment. Table 6 lists the collection of different

quantities of Ni, Cr, Mo and W at various zones of weld joint in weight percentage. The fine equiaxed dendritic structure dominates the weld center (Fig. 12a), and the interface consists of columnar dendrites (Fig. 12b). No secondary phases are observed in the interdendritic region.
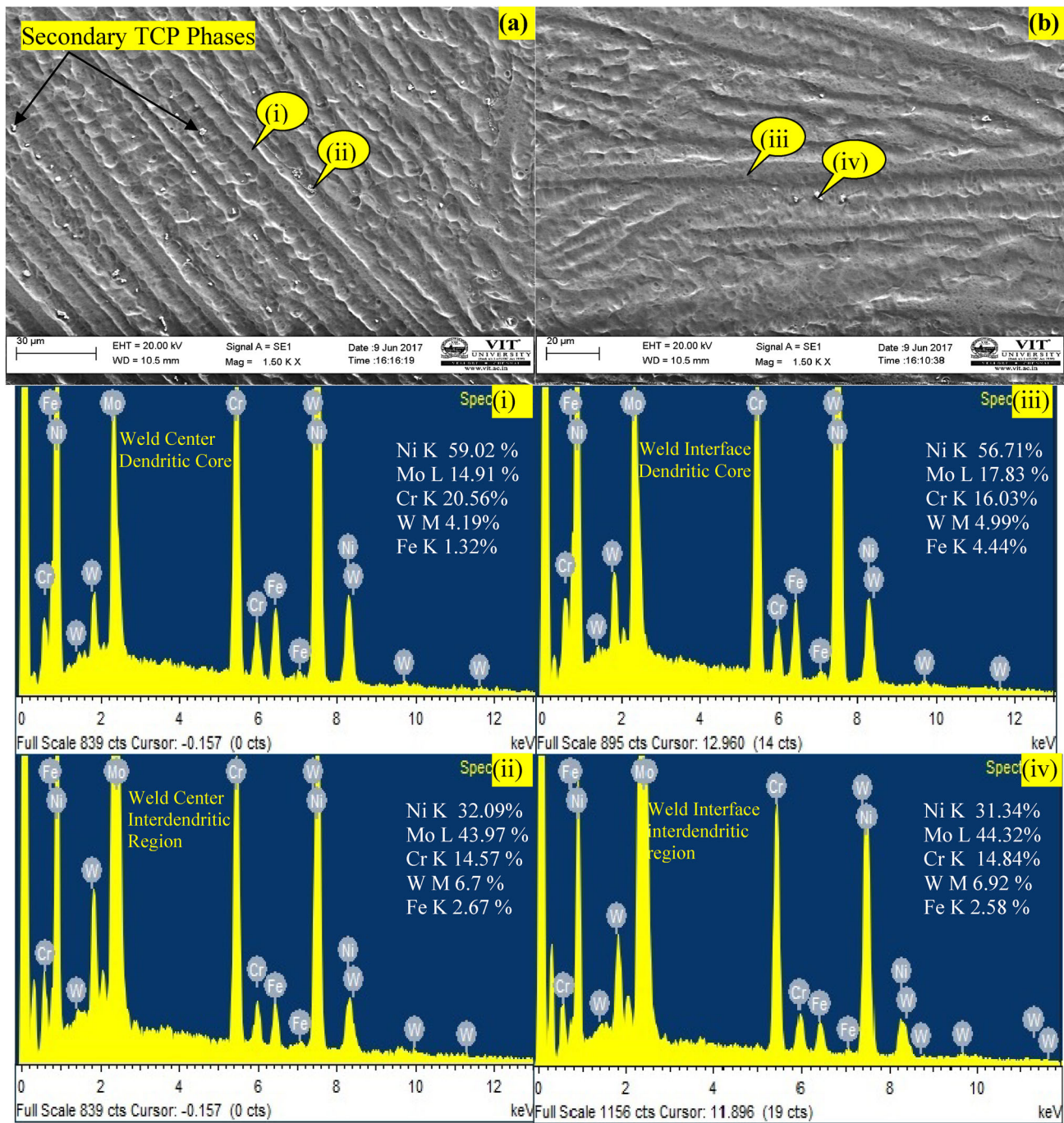
**Fig. 10** SEM/EDS analysis of PCGTA weldment fabricated with filler wire ERNiCrMo-4 of alloy 686: **a** SEM weld center; **b** SEM weld interface; (i) EDS of weld center dendritic core; (ii) EDS of weld center interdendritic region; (iii) EDS of weld interface dendritic core; and (iv) EDS of weld interface interdendritic region

EDS examination of weld center dendritic core and interdendritic regions are shown in Fig. 12i and ii. There is less difference in the elemental values of dendritic core and interdendritic region. Similar observations are also observed in the weld interface region (Fig. 12iii and iv).

### 3.4 Tensile Testing

Table 7 lists the strength and ductility of various welded joints fabricated by GTAW and PCGTAW with two different filler wires. Figure 13a–d represents the tensile failure samples of GTA and PCGTA weldments. It is

**Table 3** EDS analysis of elemental levels at different zones of GTAW-ERNiCrMo-4

| Type of welding | Zone | Ni | Mo | Cr | W | Fe |
|---|---|---|---|---|---|---|
| GTAW-ERNiCrMo-4 | Weld center dendritic core | 59.82 | 14.49 | 20.38 | 4.12 | 1.19 |
| | Weld center interdendritic zone | 34.79 | 40.91 | 16.52 | 5.76 | 2.02 |
| | Weld interface dendritic core | 61.22 | 14.76 | 19.52 | 4.00 | 0.51 |
| | Weld interface interdendritic zone | 36.42 | 39.11 | 19.33 | 4.82 | 0.32 |

**Table 4** EDS analysis of elemental levels at different zones of GTAW-ERNiCrMo-14

| Type of welding | Zone | Ni | Mo | Cr | W | Fe |
|---|---|---|---|---|---|---|
| PCGTAW-ERNiCrMo-4 | Weld center dendritic core | 59.02 | 14.91 | 20.56 | 4.19 | 1.32 |
| | Weld center interdendritic zone | 32.09 | 43.97 | 14.57 | 6.7 | 2.67 |
| | Weld interface dendritic core | 56.71 | 17.83 | 16.03 | 4.99 | 4.44 |
| | Weld interface interdendritic zone | 31.34 | 44.32 | 14.84 | 6.92 | 2.58 |

noticed from the Fig. 13 that tensile failure has occurred in the weld fusion zone in case of GTAW with ERNiCrMo-4, PCGTAW with ERNiCrMo-4 and GTAW with ERNiCrMo-14 filler wire. In case of PCGTAW-ERNiCrMo-14 weldment, the failure has occurred in the base metal. From Table 7, it is clear that PCGTAW has high ultimate strength and ductility when compared to GTAW. SEM fractography (Fig. 14a–d) contains the microvoids with shallow dimples in all cases of tensile failure samples.

### 3.5 Impact Testing

The impact toughness values of GTA and PCGTA weldments produced by filler wires ERNiCrMo-4 and ERNiCrMo-14 are shown in Table 8. The photographic images of impact-tested specimens of GTA and PCGTA weldments are presented in Fig. 15a–d. It can be seen from the picture that the impact sample did not undergo complete rupture. From Table 8, it is observed that the toughness is superior in the PCGTA weldment with matching filler wire as compared to the respective GTA weldments. SEM fractography (Fig. 16a–d) shows the microvoids with elongated dimples in all cases of impact failure samples.

## 4 Discussion

### 4.1 Weld Quality

The good-quality weld should be defect-free and without any crack. In this experimental analysis, the samples had

no defects. Figure 1 represents the welded plate photographs, and Fig. 3 shows the macrographs. The macrograph (Fig. 3a–d) reveals that the fluid flow is steady in the weld pool and represents the good welding morphology. It is observed from this investigation that there is no crack/defect identified in the welded joints. Hence, the present study confirms that the process parameters employed to fabricate 3-mm-thick alloy 686 plates are optimized. The fusion zone width of PCGTAW is comparatively lesser than that of GTAW mode. It is because of lesser confined heat input having been supplied during PCGTAW, and it is clearly indicated in Table 2. Confined heat development and multiple intermittent cooling during solidification are reasons behind obtaining smaller weld bead in PCGTAW as compared to GTAW welding [17, 19].

### 4.2 Microstructure Examination

The optical microstructure of the base metal (Fig. 4) comprised of clear grain boundaries with fine equiaxed grain structure. The grain boundaries contain annealing twins which have developed during solution treatment of the base metal [13, 20]. The microstructure/morphology of GTAW (Figs. 5, 7) predominates with cellular structure in the weld center and columnar dendrites in the weld interface zones in both filler wire cases. On the other hand, the weld joint fabricated by PCGTAW mode (Figs. 6, 8) is predominant with fine equiaxed dendrites in the weld center and columnar dendrites in the interface zone. Microstructures of PCGTA weldments are much finer than those of the GTA weldments.

In general, the rate of cooling is slower in GTAW because it holds/absorbs the continuous supply of heat
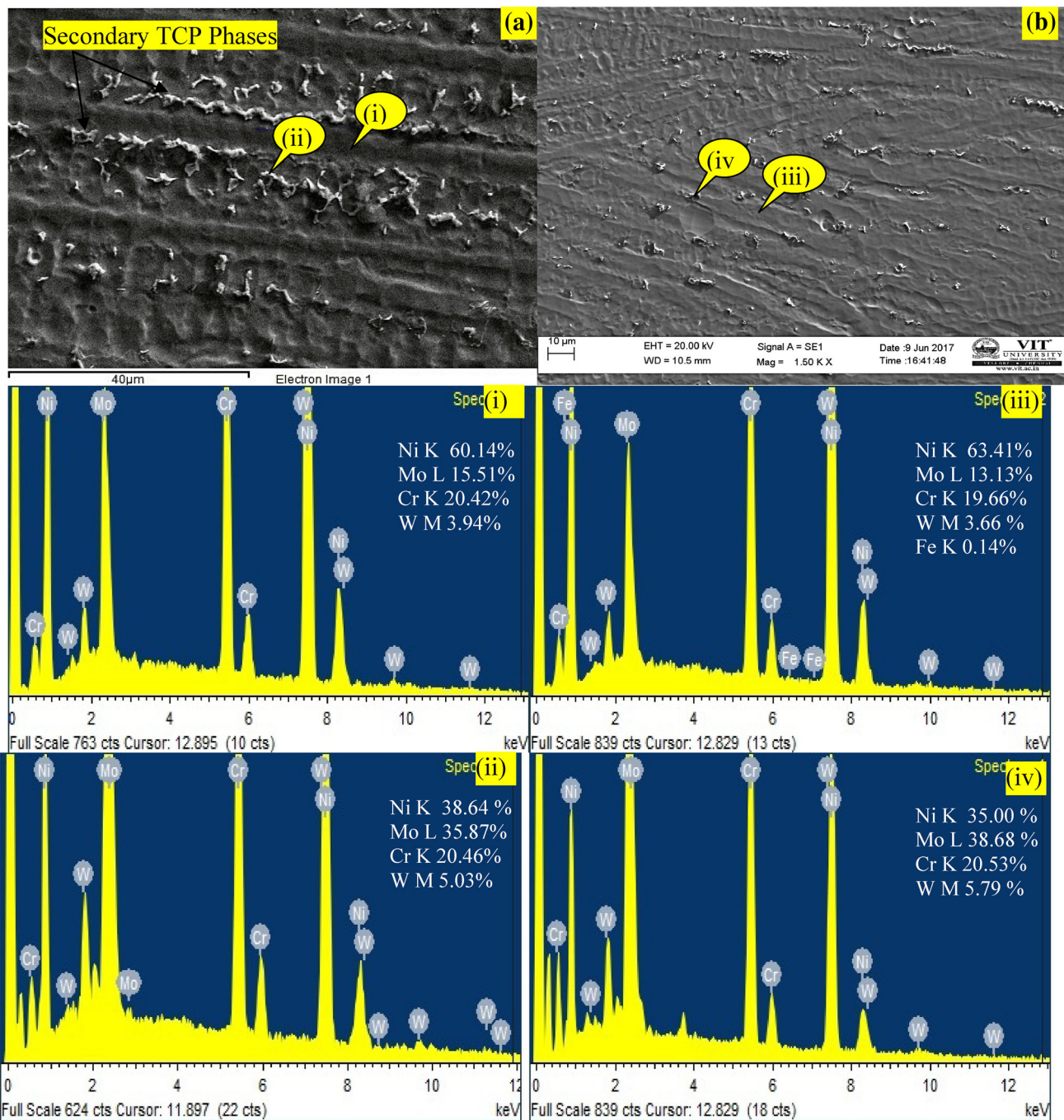
Fig. 11 SEM/EDS analysis of GTA weldment fabricated with filler wire ERNiCrMo-14 of alloy 686: **a** SEM weld center; **b** SEM weld interface; (i) EDS of weld center dendritic core; (ii) EDS of weld center interdendritic region; (iii) EDS of weld interface dendritic core; and (iv) EDS of weld interface interdendritic region

energy, which leads to the formation of the coarser microstructure. The high-temperature gradient and higher diffusion rate in GTAW never arrest the grain growth and does not allow the remelting to form the fresh grains. The scenario is different in PCGTAW which cools very fast

leading to the formation of the effective refined microstructure. Due to rapid solidification, the alloy gets solidified with lesser diffusion which activates the fresh grains to grow. Correspondingly, similar kind of refined

**Table 5** EDS analysis of elemental levels at different zones of PCGTAW-ERNiCrMo-14

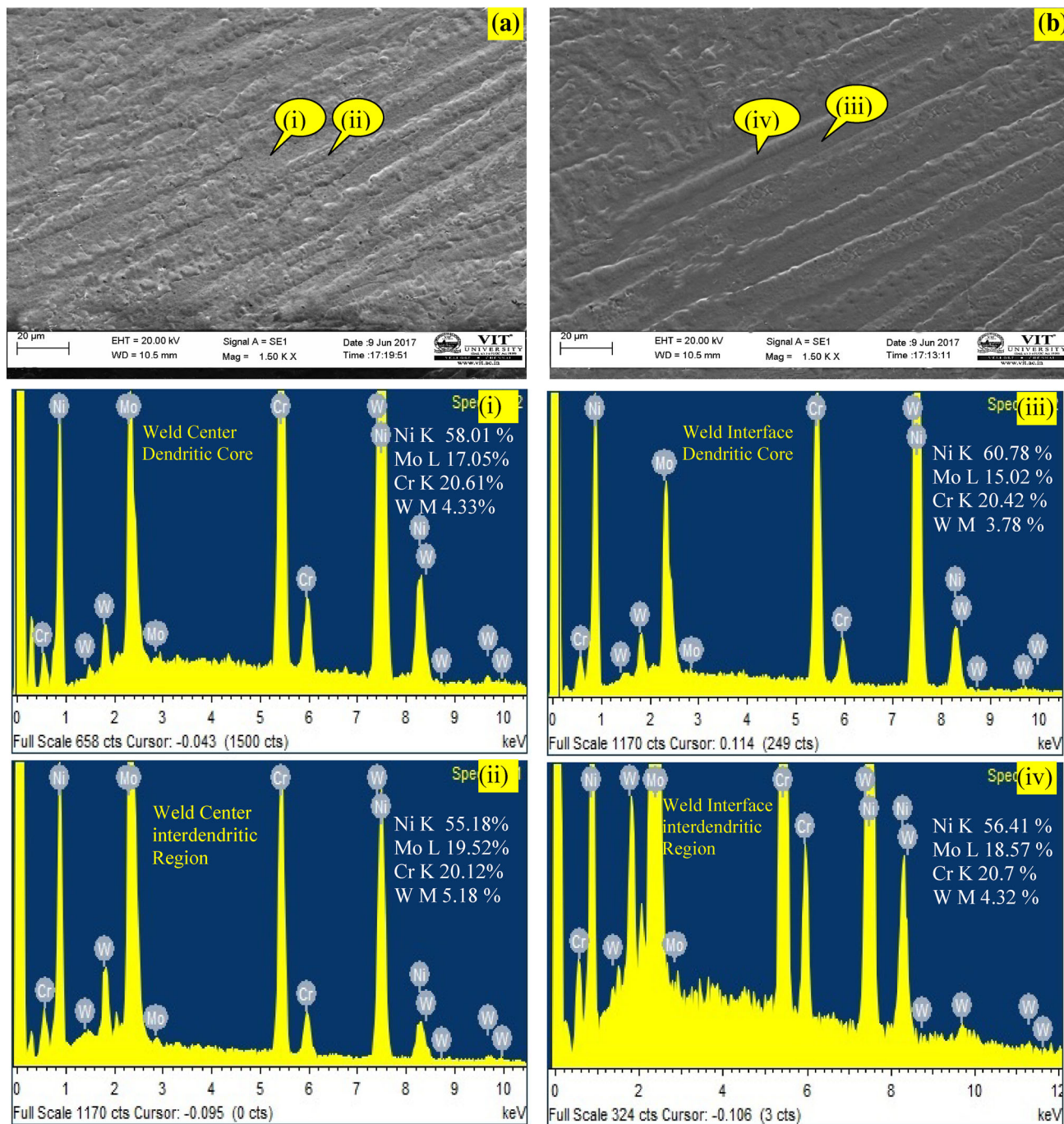| Type of welding | Zone | Ni | Mo | Cr | W |
|---|---|---|---|---|---|
| GTAW-ERNiCrMo-14 | Weld center dendritic core | 60.14 | 15.51 | 20.42 | 3.94 |
| | Weld center interdendritic zone | 38.64 | 35.87 | 20.46 | 5.03 |
| | Weld interface dendritic core | 63.41 | 13.13 | 19.66 | 3.66 |
| | Weld interface interdendritic zone | 35.00 | 38.68 | 20.53 | 5.79 |



**Fig. 12** SEM/EDS analysis of PCGTA weldment fabricated with filler wire ERNiCrMo-14 of alloy 686: **a** SEM weld center; **b** SEM weld interface; (i) EDS of weld center dendritic core; (ii) EDS of weld center interdendritic region; (iii) EDS of weld interface dendritic core; and (iv) EDS of weld interface interdendritic region

**Table 6** EDS analysis elemental levels of different zones of PCGTAW-ERNiCrMo-14

| Type of welding | Zone | Ni | Mo | Cr | W |
|---|---|---|---|---|---|
| PCGTAW-ERNiCrMo-14 | Weld center dendritic core | 58.01 | 17.05 | 20.61 | 4.33 |
| | Weld center interdendritic region | 55.18 | 19.52 | 20.12 | 5.18 |
| | Weld interface dendritic core | 60.78 | 15.02 | 20.42 | 3.78 |
| | Weld interface interdendritic region | 56.41 | 18.57 | 20.7 | 4.32 |

**Table 7** Tensile test results of GTA and PCGTA weldments fabricated with filler wire ERNiCrMo-4 and ERNiCrMo-14

| Welding process | UTS (MPa) | Average UTS (MPa) | % Of elongation | Average % of elongation | Fractured zone | % Increase/decrease from base metal |
|---|---|---|---|---|---|---|
| Base metal | 813 | 813 | 65 | 61 | – | – |
| ERNiCrMo-4 | 744 | 744 | 42 | 42 | – | – |
| ERNiCrMo-14 | 758 | 758 | 35 | 35 | – | – |
| GTAW-ERNiCrMo-4 | 805 | 808 | 45 | 46 | Fractured at weld zone | −0.61 |
| | 808 | | 46 | | | |
| | 812 | | 47 | | | |
| PCGTAW-ERNiCrMo-4 | 896 | 881 | 50 | 51 | Fractured at weld zone | 8.3 |
| | 895 | | 53 | | | |
| | 884 | | 52 | | | |
| GTAW-ERNiCrMo-14 | 853 | 866 | 46 | 47 | Fractured at weld zone | 6.5 |
| | 854 | | 47 | | | |
| | 890 | | 49 | | | |
| PCGTAW-ERNiCrMo-14 | 867 | 892 | 52 | 53 | Fractured at base metal | 9.7 |
| | 896 | | 53 | | | |
| | 880 | | 56 | | | |

grain microstructure is observed in the alloys C-276 while moving from GTAW to PCGTAW [8, 16].

In GTAW, the presence of steep temperature gradient in the weld interface region does not allow the nucleation of new grains ahead of solid-liquid interface. Further, grain which belongs to weldment only grows inside, which leads to the formation of cellular or columnar dendrite microstructure. But in PCGTAW, the temperature gradient is low and it increases the possibility of full under cooling. This provides enough driving force to solidify. Fusion zone grains grow gradually, and also nucleation of fresh grains will take place ahead of the solid–liquid interface which leads to the formation of equiaxed microstructure [21].

PCGTA welding always shows its influence in the formation of the refined microstructure. The variation of pulse current from the elevated to least level at selected frequency results in (1) cyclic variation in temperature, (2) better fluid flow, (3) faster cooling rates and (4) diminished thermal gradients in the weld pool [17].

Further, significant reduction in the size of heat-affected zone (HAZ) is also the beneficial effect of switching over from GTAW (Figs. 5b, 7b) to PCGTAW (Figs. 6b, 8b). The controlled heat input and more rapid cooling rate are responsible for the reduction of HAZ in PCGTAW. Manikandan et al. [8, 16] also obtained similar results during their work with alloy C-276.

### 4.3 SEM/EDS Analysis

From higher-magnification SEM images of GTAW (Figs. 9a, b, 11a, b), the presence of secondary phases in the interdendritic regions are clearly observed. In case of PCGTAW-ERNiCrMo-4 also, there is evidence for microsegregation (Fig. 10a, b). But from SEM images of PCGTAW-ERNiCrMo-14 (Fig. 12a, b), it is clearly observed that the formation of secondary phase is completely absent. Microsegregation is the predominant cause of premature failure of alloy 686 weldment which occurs at the end of the solidification in the fusion zone [10]. Metallurgical and mechanical properties depend on the
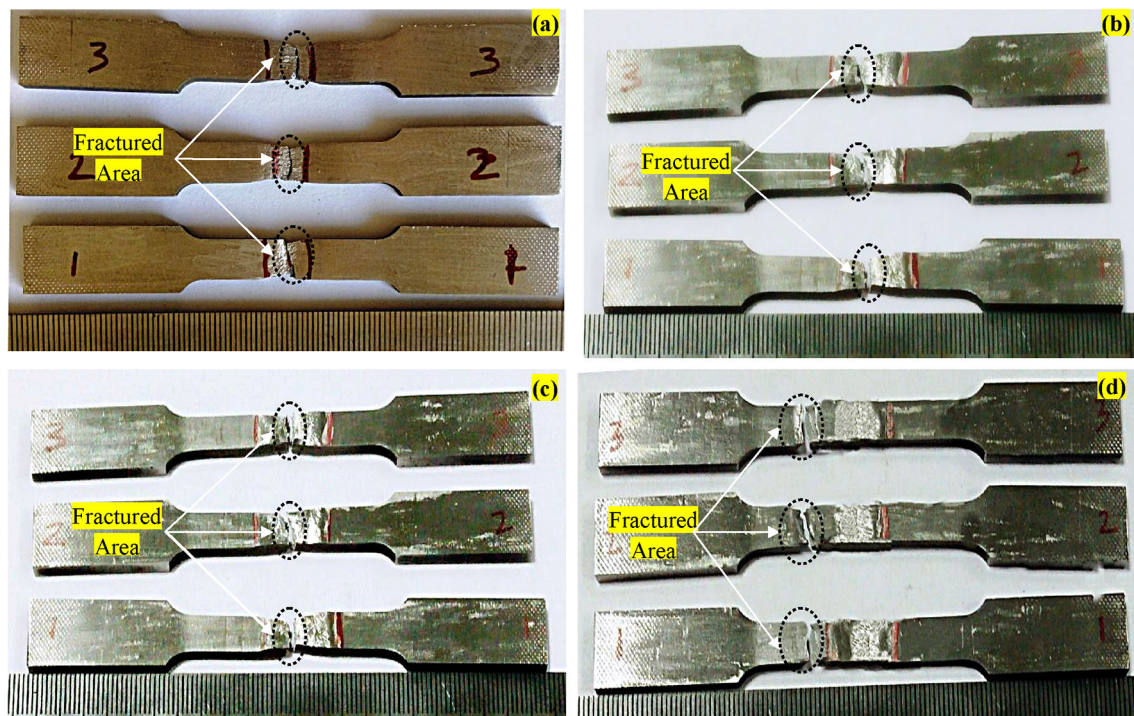
**Fig. 13** Photographs of tensile fracture samples: **a** GTAW-ERNiCrMo-4; **b** PCGTAW-ERNiCrMo-4; **c** GTAW-ERNiCrMo-14; and **d** PCGTAW-ERNiCrMo-14

amount and distribution of microsegregation in the weld joint [6]. Scheil equation is adopted in the present investigation to calculate the microsegregation of alloying elements in the present study. Many authors make use of this technique to enumerate the microsegregation of alloying element in Ni–Cr–Mo-based superalloy [8, 10], and the equation is given in Eq. (4),

$$k = \frac{C_{core}}{C_o} \tag{4}$$

where $C_{core}$ is the dendrite core elemental level and $C_o$ is the elemental level in the nominal composition of the alloy.

The distribution coefficient '$k$' is used to quantify the level of microsegregation of alloying elements during the solidification. If '$k$' value is less than 1, there is a possibility of more segregation in the interdendritic region and it ends up with the formation of secondary TCP phases. But if the value is more than 1, the segregation will be more in the dendrite core.

Table 9 represents the '$k$' values of GTAW and PCGTAW employed with two filler wires (ERNiCrMo-4 and ERNiCrMo-14). It is clearly evident in Table 9; the Mo and W elements' '$k$' value is much lower than 1, which strongly indicates severe segregation in the interdendritic region of both GTA weldments. In case of PCGTAW-ERNiCrMo-4, also Mo segregation is noted, but less than

GTAW-ERNiCrMo-4. It is because of a mismatch in chemical composition between base metal and filler wire. Manikandan et al. [8, 22] have also accounted for the same issue during their welding of alloy C-276. But '$k$' value is nearly '1' for the entire alloying element in PCGTAW-ERNiCrMo-14 weldment. This will end up in the suppression of secondary phases. The reason for Mo and W segregation in GTAW, in both filler wires, is the large amount of heat supplied during the welding (0.976 and 0.907 kJ/mm). It leads to slower cooling rate and increases the diffusion of alloying elements. Thus, it lays path to the formation of secondary TCP phases ($\mu$, P, $\sigma$) in the interdendritic region.

But in case of PCGTAW, the heat input value is lesser than PCGTAW (0.692 and 0.668 kJ/mm). It leads to minimum and nil microsegregation because it never gives sufficient time to form secondary phases. Also during solidification, the terminal liquids are broken up into several small particles.

It is noticed from the EDS analysis (Tables 3, 4, 5, 6) that the chemical composition of secondary phases observed in interdendritic regions closely correspond to the P and $\mu$ phases reported by Silva et al. [7]. Also, it was witnessed from the studies that the deleterious phases were more in GTAW weld joints and were completely absent in PCGTA welding technique using ERNiCrMo-14. It is evident from present research that the formation of
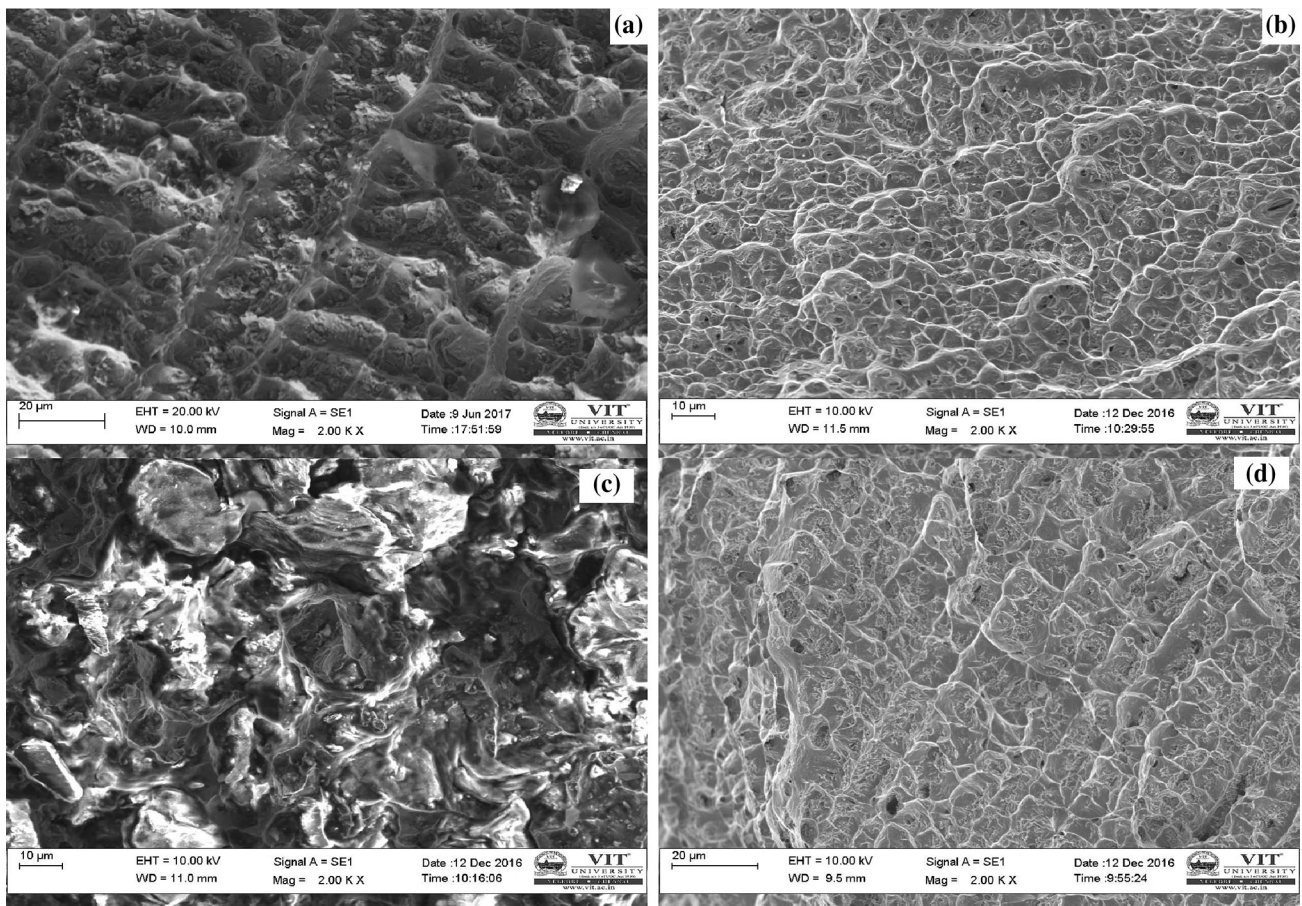
**Fig. 14** SEM fractograph of tensile failure of **a** GTAW-ERNiCrMo-4; **b** PCGTAW-ERNiCrMo-4; **c** GTAW-ERNiCrMo-14; and **d** PCGTAW-ERNiCrMo-14

**Table 8** Tensile test results of GTA and PCGTA weldments fabricated with filler wires ERNiCrMo-4 and ERNiCrMo-14

| Welding process | Toughness (J) | Average toughness (J) |
|---|---|---|
| Base metal | 43 | 43 |
| GTAW-ERNiCrMo-4 | 26 | 26 |
| | 26.5 | |
| | 25.6 | |
| PCGTAW-ERNiCrMo-4 | 32.7 | 33 |
| | 34.8 | |
| | 31.5 | |
| GTAW-ERNiCrMo-14 | 36.5 | 36.3 |
| | 35.2 | |
| | 37.4 | |
| PCGTAW-ERNiCrMo-14 | 37 | 37 |
| | 38.5 | |
| | 35.4 | |

secondary phases in the pulsed current with matching filler wire composition is completely suppressed.

The main reason for microsegregation of alloying elements particularly Mo and W is the variation in atomic radii between Ni (solvent) and other alloying elements (solute). The atomic radius difference between Ni and Mo is 9%. The atomic radius difference between Ni and W is 10%. But other elements (Cr and Fe) size difference with
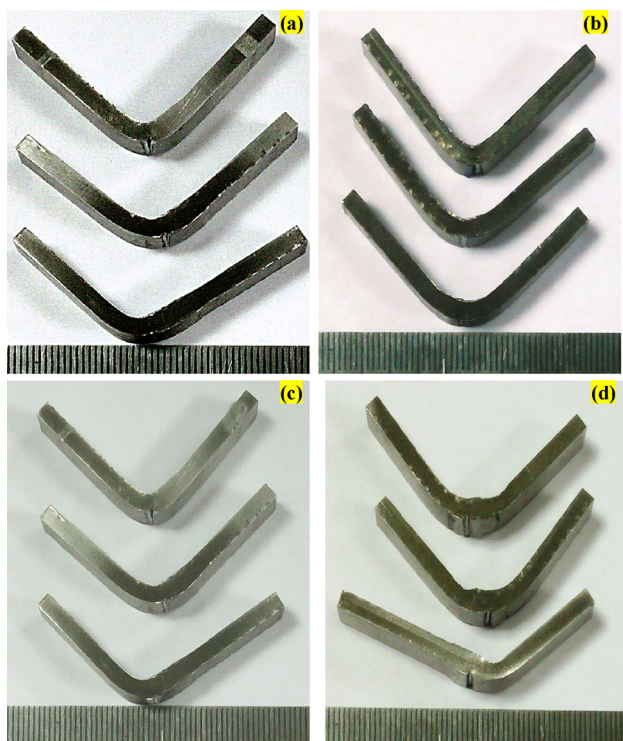
Fig. 15 Photographs of impact fracture samples: **a** GTAW-ERNiCrMo-4; **b** PCGTAW-ERNiCrMo-4; **c** GTAW-ERNiCrMo-14; and **d** PCGTAW-ERNiCrMo-14

Ni is very less (1%) and has minimum effect on microsegregation [6]. It is well matched with 'k' values of the present study given in Table 9.

### 4.4 Tensile Test

Tensile studies report that the fracture has occurred at the weld zone in all the trials except PCGTAW-ERNiCrMo-14 weldment. The microsegregation and secondary phase formation are responsible for weld zone fracture. The absence of secondary phase formation results in base metal tensile fracture in case of PCGTAW-ERNiCRMo-14. From tensile test results, it is clear that tensile properties of PCGTA weld joints are considerably higher than those of GTAW welds. It is also observed that there is an increase in ultimate tensile strength of GTA and PCGTA weldments than the base metal except for GTAW-ERNiCrMo-4. Severe microsegregation is considered to be the reason for this particular weld joint. These results are inline with the results of SEM/EDS analysis as discussed in Sect. 4.3. Dupont et al. [6] have accounted for that the mechanical properties will be diminished with the formation of secondary phases in Ni–Cr–Mo-based superalloy weld joints. Tensile fractography analysis (Fig. 14a–d) indicates the coalescence of microvoids and shallow dimples which are

scattered at the fibrous fractured zone. This confirms the ductile mode of failure in all four weld joints.

### 4.5 Impact Test

Table 8 indicates the impact toughness results acquired from the present study. Impact assessments on the alloy 686 weldments clearly indicates (Table 8) that the impact toughness of PCGTAW-ERNiCrMo-14 weldment (37 J) has been found to be better compared to GTA weldments (26 and 36.3 J). The impact toughness value GTAW-ERNiCrMo-4 is the least among other weldments involved in this present study, and it is due to the mismatching of chemical composition between the base metal and particular filler wire. The refinement in microstructure and minimum/nil microsegregation at PCGTA welding is the reason behind the improvement in impact toughness when switching over from GTAW to PCGTAW. The reduction in the toughness of the weldment compared to the base metal is the due to the formation of secondary phase precipitates in the fusion zone [6].

Figure 15a–d shows that the impact samples are unbroken in all four weld samples. Hence, it is proved that the mode of failure is ductile in the entire weld joints employed in this study. From the SEM fractography (Fig. 16a–d), it is evident that the presence of microvoids and dimple have resulted in the ductile mode of failure. It is found from the impact studies that the PCGTA weldments employing ERNiCrMo-14 offer better resistance against sudden impact load.

### 4.6 Recommended Welding Technique

The present research work suggests that weld joint fabricated by pulsed current mode with filler wire (ERNiCrMo-14) renders better results in terms of enhancement in the microstructure, the absence of microsegregation and enhanced mechanical properties. So, it can be chosen as the best weldment out of four welded joints employed in the present study.

## 5 Conclusions

Based on the research work the following conclusions are drawn:

- Macro-examination confirmed that the weldments fabricated with GTAW and PCGTAW employed with two different filler wires were defect-free and this indicated precise weld process parameters used in the present study.
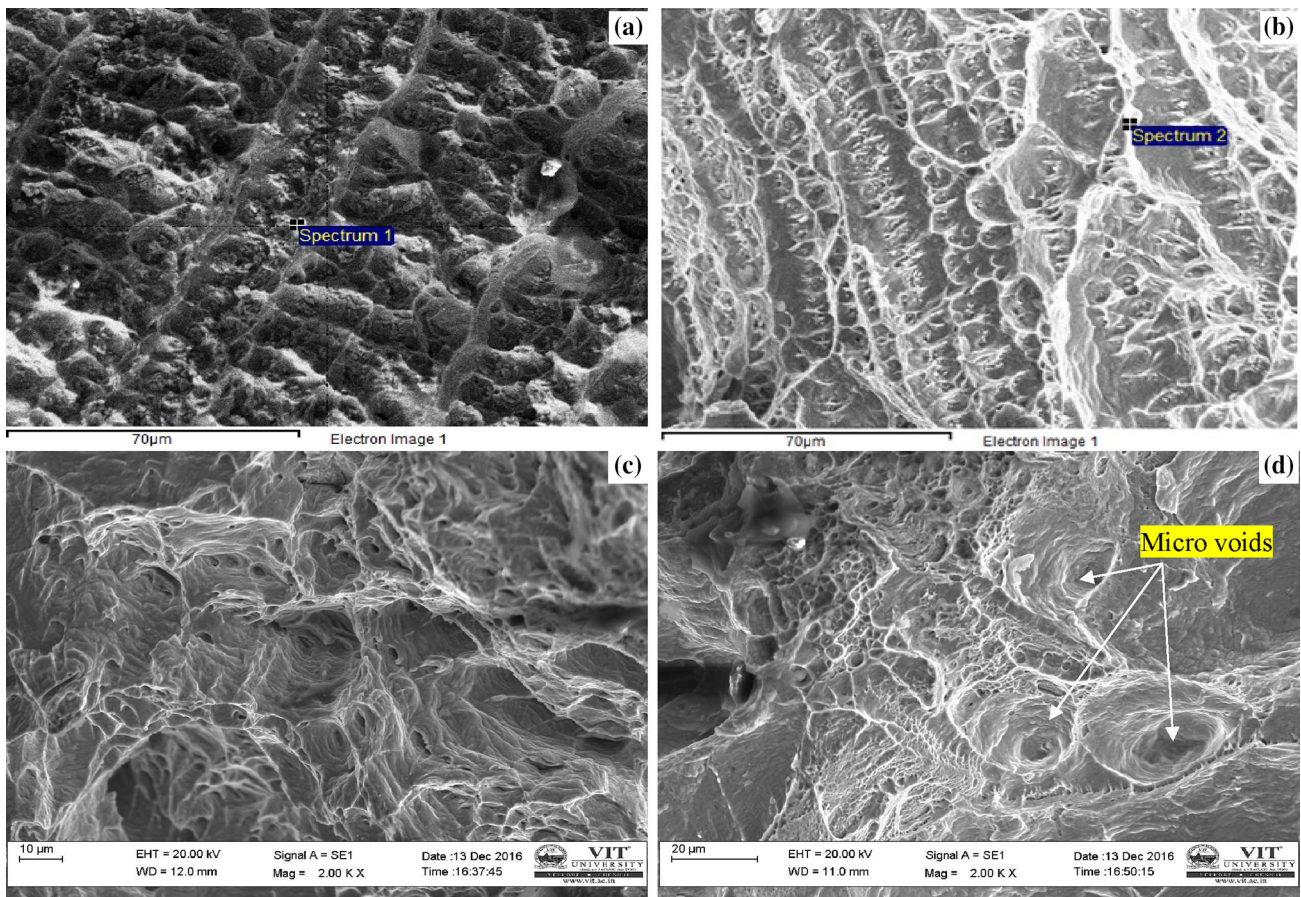
**Fig. 16** SEM fractograph of impact failure of **a** GTAW-ERNiCrMo-4; **b** PCGTAW-ERNiCrMo-4; **c** GTAW-ERNiCrMo-14; and **d** PCGTAW-ERNiCrMo-14

**Table 9** Distribution coefficient ($k$) values of alloying elements in GTA and PCGTA welded with different filler wires of alloy 686

| Type of welding | Ni | Mo | Cr | W |
|---|---|---|---|---|
| GTAW-ERNiCrMo-4 | 1.08 | 0.76 | 0.98 | 0.85 |
| PCGTAW-ERNiCrMo-4 | 1.07 | 0.79 | 0.99 | 0.86 |
| GTAW-ERNiCrMo-14 | 1.09 | 0.82 | 0.98 | 0.81 |
| PCGTAW-ERNiCrMo-14 | 1.05 | 0.90 | 0.99 | 0.89 |

- All PCGTAW weld joints employed in this study revealed narrower weld bead width and small-sized HAZ which were due to the effective/lower heat input during current pulsing when compared to GTAW.
- The fusion zone weld center microstructure of PCGTAW with filler wires (ERNiCrMo-4 and ERNiCrMo-14) was decorated with fine equiaxed dendrite structure. But in case of GTAW, the fusion zone microstructure was extended with coarser microstructure. The faster cooling rates available in PCGTAW were generally accountable for the refinement in the microstructure.

- SEM/EDS analysis revealed the occurrence of secondary phases in the interdendritic regions of GTAW—both filler wires and PCGTAW-ERNiCrMo-4 filler wire. The microsegregation was high in GTAW and absent in PCGTAW-ERNiCrMo-14. The slower cooling rate and continuous heat supply during GTAW resulted in severe microsegregation which laid the path to the formation of higher amount of secondary phases.
- The tensile and impact test results revealed that PCGTAW showed marginally enhanced mechanical properties in terms of strength, ductility and toughness when compared to GTAW. The reason for the improvement in properties of PCGTAW was the refined

microstructure and the minimum of secondary phases in the interdendritic region.

**Compliance with Ethical Standards**

**Conflict of interest** The authors declare that they have no conflict of interest.

**Human and Animal Rights** This article does not contain any studies with human or animal subjects.

# References

1. Shoemaker L E, Crum J R, Nickel–chromium–molybdenum superalloys: the solution to corrosion problems in wet limestone FGD air pollution control systems http://www.pccforged products.com/web/user_content/files/wyman/Ni%20Cr%20Mo% 20Alloys%20-%20Solution%20to%20Corrosion%20problems% 20in%20Wet%20Limestone%20FGD%20Air%20Pollution%20 Control%20 Systems.pdf; 2014. Accessed 08 August 2016.
2. Shoemaker L E, Crum J R, Experience in effective application of metallic materials for construction of FGD systems, Spec. Met. Tech. data Sheet, http://pccforgedproducts.com/web/user_ content/files/wyman/Metallic%20Materials%20for%20Construc tion%20of%20FGD%20Systems.pdf; 2015. Accessed 08 August 2016.
3. Special Metal Data Sheet, Alloy 686, http://www.special-metals.de/files/INCONEL%20alloy%20686.pdf. Accessed 08 August 2015.
4. Special Metal Data Sheet, http://www.specialmetalswiggin. co.uk/pdfs/products/INCONEL%20alloy%20686.pdf. Accessed 08 August 2016.
5. Shoemaker L E, Crum J R, Spec. Met. Tech. Data Sheet http://www.pccforgedproducts.com/web/user_content/files/wym an/Corrosion%20Performance%20and%20Fabricability%20of% 20the%20New%20Generation%20of%20Highly%20Corrosion %20Resistant%20NiCrMo% 20Alloys.pdf; 2015. Accessed 08 August 2015.
6. Dupont J N, Lippold J C, and Kiser S D, *Welding Metallurgy and Weldability of Nickel-Base alloys,* Wiley, Hoboken (2009) p 47.
7. Silva C C, Afonso C R M, Ramirez A J, Motta M F, Miranda H C, and Farias J P, *J Alloys Comp* **684** (2016) 628.
8. Manikandan M, Arivazhagan, N, Nageswara Rao M, and Reddy G M, *Acta Metall Sinica* **28** (2015) 208.
9. Crum J R, and Shoemaker L E, Special Alloys and Overmatching Welding Products Solve FGD Corrosion Problems, Special Metals Technical data sheet http://216.71.103.52/documen ts/Special%20Alloys%20and%20Overmatched%20Welding%20 Products%20Solve%20FGD%20Corrosion%20Problems.pdf 2015. Accessed 08 August 2015.
10. Arulmurugan B and Manikandan M, *Mater Sci Eng A*, **A69** (2017) 126.
11. Cieslak M J, Headley T J, and Romig A D, *Metall Trans A* **17A** (1986) 2035.
12. Perricone M J, and DuPont J N, *Metall Mater Trans A* **37A** (2006) 1267.
13. Zheng Y R, *Acta Metall. Sinica* **35** (1999)12.
14. Gallagher M L, and Lippold J, in *Hot Cracking Phenomena in Welds III*, (eds) Lippold J, Bollinghaus T, Cross C, Springer, New York (2011), p 367. https://doi.org/10.1007/978-3-642-16864-2.
15. Manikandan S G K, Sivakumar D, Prasad Rao K, and Kamaraj M, *J Mater Process Technol* **214** (2014) 358.
16. Manikandan M, Arivazhagan N, Nageswara Rao M, and Reddy G M, *J Manuf Processes* **16** (2014) 563.
17. Janaki Ram G D, Venugopal Reddy A, Prasad Rao K, and Madhusudhan Reddy G, *Sci Technol Weld Join* **9** (2004) 390.
18. Farahani E, Shamanian M, and Ashrafizadeh F, *AMAE Int. J Manuf Mater Sci* **02** (01) (2012) 1.
19. Manikandan M, Nageswara Rao M, Ramanujam R, Ramkumar D K, Arivazhagan N, and Reddy G M, *J Procedia Mater Sci* **97** (2014) 767.
20. Yousefieh M, Shamanian M, and Arghavan A R, *J Metallogr Microstruct Anal* **1** (2012) 85.
21. Kou S, *A Textbook on Welding Metallurgy*. Wiley, New Jersey, (2003) p 170.
22. Manikandan M, Arivazhagan N, Arivarasu M, Mageshkumar K, Rajan D N, Murugan B A, Prasanth P, Sukumar S, and Vimalanathan R, *Trans Indian Inst Met* **70** (2017) 661.